PERGAMON

Atmospheric Environment 36 (2002) 5795–5806

ATMOSPHERIC ENVIRONMENT

www.elsevier.com/locate/atmosenv

Characterization of ultrafine and fine particles at a site near the Great Smoky Mountains National Park ☆

Meng-Dawn Cheng[a,*], Roger L. Tanner[b]

[a] *Oak Ridge National Laboratory, Environmental Sciences Division, Building 1505, Mail Stop 6038, P.O. Box 2008, Oak Ridge, TN 37831-6038, USA*

[b] *Tennessee Valley Authority, Environmental Research Center, Muscle Shoals, AL 35662, USA*

Received 7 March 2002; accepted 19 July 2002

Abstract

Continuous measurements were taken during a 22-day campaign held in the summer of 2000 at a site close to the Great Smoky Mountains National Park in eastern Tennessee. The campaign was conducted to investigate the relationships between ultrafine/fine particles and gaseous species observed. A varimax-rotation factor analysis was performed to explore the relationship of the fine and ultrafine particle number concentrations, the gaseous species concentration, the mean wind speed, and the solar radiation. A 6-factor model was found to best resolve 79.7% of the variability embedded in the data. The model suggests that 31.4% of the data variability could be explained by ultrafine particles (the diameters smaller than or equal to 100 nm). It was difficult to label this factor without chemistry information of the ultrafine particles. However, no gas species were loaded on Factor 1 indicating the ultrafine particles observed in this study were not associated with primary source emissions. The decoupling of the ultrafine particles from the fine particles also implies that the former ones might have been produced and transported to the site by separated mechanisms from those of fine particles. The second factor included the $PM_{2.5}$ mass concentration and the number concentrations of particles in the diameter range of 101–400 nm. The loading pattern on Factor 2 led to the conclusion that this factor was contributed by regional transport. The third factor includes CO, NO_2, reactive odd nitrogen (NO_y), and SO_2 that were contributed by primary source emissions. The mean wind speed and ozone were loaded in Factor 4 that was labeled as ozone transport. Identification of this factor led to an observation that ozone transport to the site was essentially decoupled from the regional transport factor of fine particles (i.e., Factor 2). Solar radiation was singly included in the fifth factor indicating this is a unique factor. The quality of NO data was marginal and the variable was distilled by the model into Factor 6. A multiple regression analysis further indicated that $PM_{2.5}$ mass concentration was best explained by CO, O_3, and number concentrations of particles in the diameter range between 0.1 and 0.4 μm. We also identified two unique events during the campaign in which the number concentrations of 31–51 nm particles dramatically increased by a factor of 10 in 30 min, reaching 40,000 cm^{-3} and lasting for a couple of hours. Particles in the size range just below and above those in the 31–51 nm diameter range also exhibited increases during these events, but the changes were much less dramatic.

Keywords: The Great Smoky Mountains National Park; Factor analysis; Ultrafine and fine particles; Source–receptor relationships

*Corresponding author. Tel.: +1-865-241-5918; fax: +1-865-576-8646.

E-mail address: chengmd@ornl.gov (M.-D. Cheng).

1352-2310/02/$ - see front matter
PII: S1352-2310(02)00625-8

1. Introduction

Most of the ambient particles in urban atmospheres are in the ultrafine size range (Peters et al., 1997; Woo et al., 2001), that is, with diameters <100 nm ($=0.1$ μm). Ultrafine particles have been observed during photochemical and nitrate radical reactions in outdoor smog chambers (cf., Heisler and Friedlander, 1977; McMurry and Friedlander, 1979; Flagan et al., 1991). Wehner et al. (2000) observed high levels of ultrafine particles during the millennium fireworks display in Germany. Ultrafine particles have also been measured in remote areas such as the tropical boundary layer (Clarke, 1992) and in polar areas (Pirjola et al., 1998). Production of particles via nucleation in a boreal forest was studied in an EU funded project BIOFOR and has been reported in several recent articles published at *Tellus* 53B(4) in 2001. Inorganic compounds and hygroscopic organic compounds contributed to the particle growth during daytime, while organic compounds comprised a major fraction of the ultrafine particles at nighttime in Southern Finland (Kulmala et al., 2001).

In the eastern US, sulfate constitutes the largest mass fraction of summertime fine particles. On average, the chemical composition of fine airborne particulate matter at Look Rock in summer was approximately 56% ammonium sulfates, 30% organic carbon, 6% elemental carbon, 0.4% ammonium nitrate, and the remaining fraction ($\cong 7\%$) undetermined (Tanner and Parkhurst, 2001). The Great Smoky Mountains National Park (GSMNP) in eastern Tennessee is a Class I region, and has been visited annually by more than 10 million people during the past few years, making it the most popular national park in the continental United States. Mobile source emissions from nearby urban areas (for example, Knoxville) and interstate highways (I-40, I-75, I-81), and stationary source emissions from industrial activities and coal-fired power plants are potential contributors of pollutants to the park. These sources emit precursor gases such as nitrogen oxides (NO_x), sulfur dioxide (SO_2), carbon monoxide (CO), and possibly hazardous air pollutants. Forested areas in the GSMNP give off a series of biogenic organic compounds (principally isoprene) as well as water vapor. The combination of man-made and biogenic emissions and abundant sunshine and water vapor leads to summertime production rates and levels of ultrafine particles that are relatively high in the vicinity of the GSMNP. We report atmospheric measurement of number concentration and size distribution of ultrafine/fine particles and various gaseous species taken at a site near the GSMNP during the summer of 2000.

2. Experimental

During a 4-week intensive field campaign in the summer of 2000, a number of measurements were made continuously at Look Rock, Tennessee, a sampling site operated by the Tennessee Valley Authority (TVA) and collocated with the IMPROVE network site operated by the National Park Service (NPS). The Look Rock air quality monitoring station is located in a rural area in Blount County, TN (see Fig. 1) at 35.6°N, 83.9°W, and 793 m above mean sea level. The land use pattern at the site is predominantly mixed deciduous forest. On-site meteorological measurements during the field campaign included wind speed, direction, solar radiation, temperature, and precipitation. A real-time camera is used to photograph vistas every 15 min, and current photos can be seen on-line at: http://www2.nature.nps.gov/ard/parks/grsm/Lookrockweather.htm along with the archived photo for 1500 h of each day.

TVA measurements included the following gaseous species: nitrogen oxide (NO), NO_2, NO_y, SO_2, O_3, and CO. Aerosol mass composition was measured on filter samples collected using two collocated Federal Reference Method samplers, and by a PC-BOSS sampler (Modey et al., 2001; Ding et al., 2002) which quantified semi-volatile as well as non-volatile organic aerosol components. A TEOM continuous $PM_{2.5}$ mass monitor was also operated by TVA personnel during this period. The size distribution of particles of diameter between 15 and 626 nm was taken on a continuous basis using a TSI Model 3080 scanning mobility particle spectrometer (SMPS) operated by Oak Ridge National Laboratory (ORNL) personnel. The observable parameters are listed in Table 1, and the sampling frequencies of these measurements are also described in the table.

Measurements of particle size distribution were made using the SMPS equipped with a differential mobility analyzer (LDMA) and an ultrafine condensation particle counter (TSI, 3025A). The ratio of sheath to aerosol flow rates used in the LDMA was 10:1 during the campaign. A 0.0457-cm impactor disc was in place at the aerosol inlet on the TSI 3080 classifier. The up-scan time was 240 s and the down-scan time 60 s for each size spectrum that corresponds to an acquisition time of 5 min per size spectrum. There were a total of six scans in each 30-min averaged sample size distribution measurement. An aerosol inlet was placed at 3 m above a sampling deck that is located above the roof of the TVA sampling enclosure. A 1.27-cm ID sampling tube, 7 m in length was used to connect the inlet to the instrument. Four meters of the tube length was stainless steel, while the remaining length was PE with a 1.25 cm ID. Ambient particles were drawn at a flow rate of $10\,l\,min^{-1}$ passing through a dryer, with $0.3\,l\,min^{-1}$ of the flow sampled by the SMPS at T, and the excess flow, filtered by an in-line HEPA filter, vented back to the

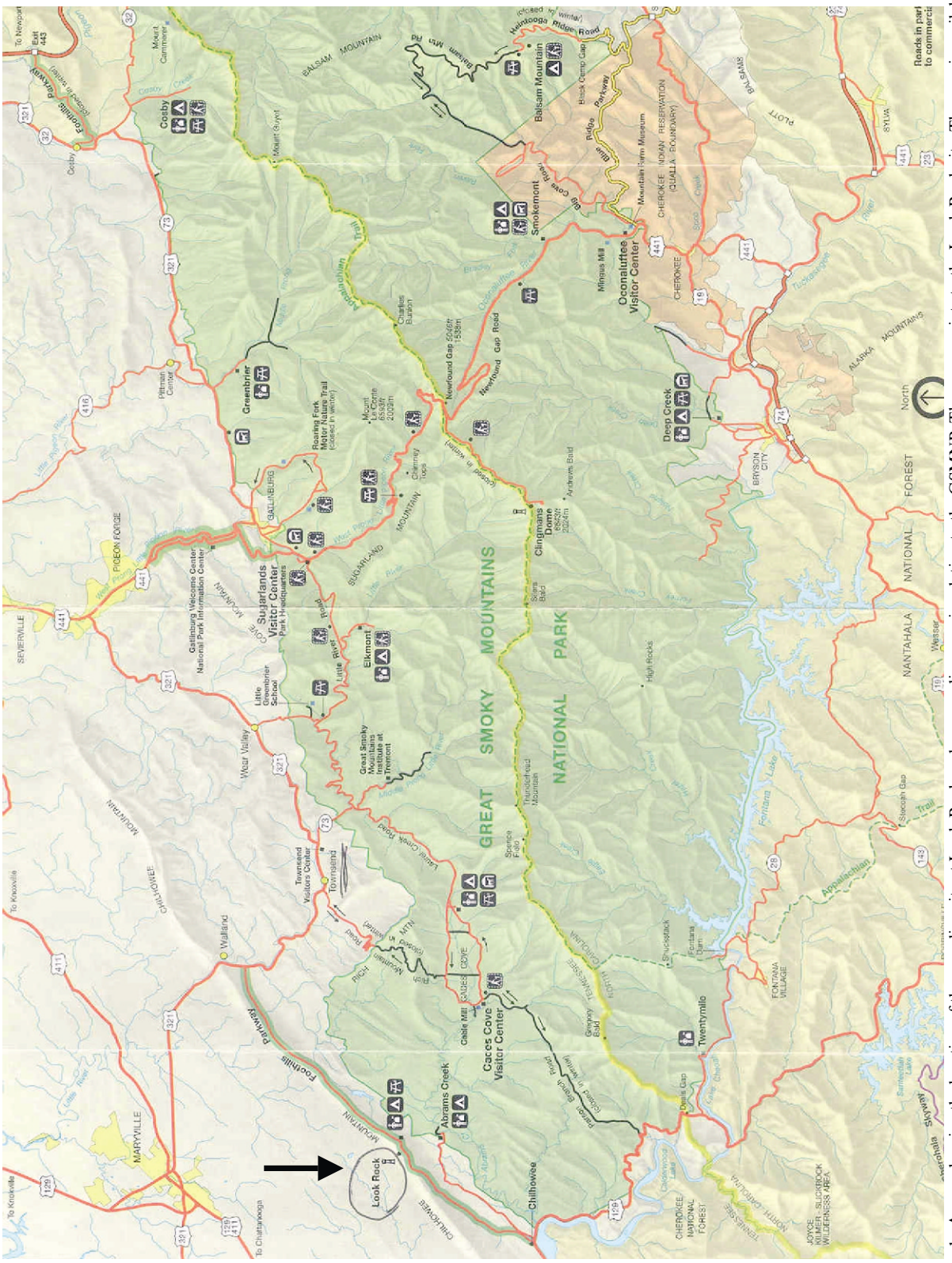

Fig. 1. A map showing the location of the sampling site at Look Rock and surrounding area in relation to the GSMNP. The arrow points to the Look Rock site. The map is available to the public at the Sugarland visitor center in the park.

Table 1
Summary of continuous measurements

Parameters	Interval (min avg.)	Instrument	Comments
Ozone, O_3	1	TEII 49	Full-scale range: 0–200 ppb; zero: Clean, dry air; Span: 160 ppb; precision: 40 ppb; Time constant: 30 s
NO/NO_2	1	TEII 42S	Full-scale range: 0–50 ppb; span (w/NO): 20 ppb; Addition (w/NO) 3 ×: 5 ppb; zero: night readings; Time constant: 10 s
NO_y	1	TEII 42S	Full-scale range: 0–100 ppb; span (w/NO): 40 ppb; Addition (w/NO) 3 ×: 10 ppb; Addition (w/NPN) 3 ×: 50 ppb; Zero 4 ×: clean dry air; time constant: 10 s
CO	1	TEII 48S	Full-scale range: 0–1000 ppb; span: 800 ppb; Addition (w/CO) 2 ×: 200 ppb; Zero 12 ×: ambient native zero gas Time constant: 20 s
SO_2	1	TEII 43S	Full-scale range: 0–100 ppb; Addition (w/SO_2) 2 ×: 20 ppb; Zero 2 ×: clean dry air; time constant: 20 s Full-scale voltage output: 10 V
Wind speed	1	R.M. Young	10 m above ground
Wind direction	1	R.M. Young	10 m above ground
Air temperature	1	Platinum RTD	10 m above ground
Humidity	1	Rotronics	10 m above ground
Total UV radiation	1	Eppley	9 m above ground
Particle size distribution	6	TSI SMPS 3080LDMA	Inlet at 10 m above ground, data in # cm^{-3}.

atmosphere. The relative humidity in the aerosol stream was lower than 40%. The SMPS instrument was located inside the climate-controlled TVA enclosure that maintained the air temperature at a constant 21°C.

Individual 1/4″ OD Teflon sampling lines are used to deliver the NO/NO_2 and NO_y samples to their respective monitors housed also inside the trailer. The NO and NO_2 are sampled through a common sampling line that is then split to pass either through a photolytic cell or pass directly into the TEII 42S instrument which has its converter removed. The NO_y converter from the TEII 42S is placed within the inlet box placed at a height of 10 m and operated at 350°C. A dedicated line runs from the converter to the second TEII 42S to obtain NO_y measurements. Teflon lines have been installed to allow for introduction of the standard gas mixture, output from a standard addition system, and zero air at the sample intakes during span and zero procedures and during calibration.

The site is equipped with a TEII Model 111 Zero Air generating system and a modified TEII 146 Dynamic Gas Calibrator. The TEII 146 is modified to allow gas addition method span checks for the NO, NO_2, and NO_y gas monitors using individual cylinders of NO, NO_2, and *n*-propyl nitrate (NPN) gas standards. The NO_y converter efficiency was checked daily by the gas addition of NPN and weekly by gas addition of HNO_3. Calibrations are conducted at the start and end of the study, or more frequently if instrument performance requires calibration. Calibrations are conducted on the NO_x–NO_y analyzers using an ESE-built gas dilution system that has been modified by TVA and integrated to a TEII 146 Dynamic Gas Calibrator using NIST traceable gas cylinders of NO. EPA Protocol NO_2 gas cylinder from Scott Specialty Gas is used to determine the NO_2 photolytic cell conversion efficiency. The catalytic converter on the NO_y measurement systems is checked using NPN obtained from Scott Marrin. Calibrations are conducted through the sampling inlets using gas substitution methods and consist of a zero reading and four upscale points with three points in the ambient measurement range. The EPA-certified TEOM instrument with a 2.5 μm cyclone inlet and humidity control was used to perform 5-min averaging fine particle mass concentration measurements using its own dedicated sampling line. The TEOM was operated at 30°C with a non-commercial Nafion dryer for humidity control.

3. Results and discussion

The data recovery rates were between 48% and 71%; the number of 30-min averaged data points for the measured variables ranged from 502 to 744 during the 22-day 2000 summer campaign (JD 230 to JD 252, see

Table 2
Summary statistics of variables

	Counts	Average	Standard deviation	Max	Min	Median	Upper quartile	Lower quartile	Data recovery (%)
Σ(15–30)	744	1059	2834	49806	0	407	861	201	70
Σ(31–40)	744	2175	5049	94743	136	932	2421	532	70
Σ(41–50)	744	3059	6225	92042	274	1440	3182	855	70
Σ(51–60)	744	3925	5262	66579	373	2418	4230	1640	70
Σ(61–100)	744	10612	6723	51770	1410	9354	12262	6232	70
Σ(101–200)	744	14133	8721	47743	2765	11049	19505	7846	70
Σ(201–400)	744	7732	4640	21998	1102	6305	9696	4712	70
Σ(401–626)	744	1527	965	8614	48	1445	1912	923	70
$PM_{2.5}$ mass	698	7.98	5.32	30.97	0.66	6.62	9.77	4.46	66
O_3	716	52.38	14.78	87.05	16.63	51.51	63.24	41.10	68
SO_2	746	1.20	1.88	21.11	0.00	0.57	1.56	0.20	71
CO	739	171	42	441	79	169	195	144	70
NO	502	0.11	0.58	8.37	0.00	0.03	0.09	0.01	48
NO_y	730	3.23	1.80	19.09	0.77	2.87	3.93	2.02	69
NO_2	573	0.98	0.88	6.94	0.02	0.68	1.06	0.51	54
Mean wind speed	746	2.54	0.76	6.22	1.23	2.45	3.00	1.96	71
Radiation	745	179	248	931	0	19.5	321.78	0.00	71

Note: Σ(A–B) = sum of number concentrations of particles in the size range of A–B nm, in units of cm^{-3}, $PM_{2.5}$ mass = $PM_{2.5}$ mass concentration, $\mu g\,m^{-3}$; CO = carbon monoxide, ppbv; O_3 = ozone, ppbv; NO = nitrogen oxide, ppbv; NO_2 = nitrogen dioxide, ppbv; NO_y = reactive nitrogen, ppbv; SO_2 = sulfur dioxide, ppbv; mean wind speed = $m\,s^{-1}$; radiation = $W\,m^{-2}$.

Table 2). To summarize the center of the distribution of air quality variables, we report the median value because of the skewed distribution of the data. The 30-min median $PM_{2.5}$ mass concentration (averaged from 5-min TEOM measurements) was $6.6\,\mu g\,m^{-3}$ ranging from 0.7 to $31\,\mu g\,m^{-3}$. The median concentrations for gases in ppbv (ranges in parentheses) were O_3: 51.5 (17–87); SO_2: 0.6 (below detection limit to 21); NO_y: 2.9 (0.8–19); NO: 0.03 (below detection limit to 8.4); NO_2: 0.7 (0.02–6.9). Measured particle number concentrations, $dN/d\log(D_p)$, were summed into larger bin sizes as 15–30 nm [denotes Σ(15–30)], 31–40 [Σ(31–40)], 41–50 [Σ(41–50)], 51–60 [Σ(51–60)], 61–100 [Σ(61–100)], 101–200 [Σ(101–200)], 201–400 [Σ(201–400)], and 401–626 [Σ(401–626)] nm. The median number concentrations were 407, 932, 1440, 2418, 9354, 11049, 6350, 1445 cm^{-3} for the summed size bins, respectively. The 30-min median wind speed was $2.5\,m\,s^{-1}$ ranging from 1.2 to $6.2\,m\,s^{-1}$.

3.1. Time series of observed variables

The time series of 30-min TEOM $PM_{2.5}$ mass concentration is shown in Fig. 2. The $PM_{2.5}$ mass reached $31\,\mu g\,m^{-3}$ at the beginning of the campaign on Julian Day (JD) 231 around mid-night (00 local standard time, LST) then decreased to as low as $16\,\mu g\,m^{-3}$ at the noon of JD 231. There were some invalid data between JD 232 and JD 233. TEOM $PM_{2.5}$ mass concentration (*$PM_{2.5}$ mass hereafter*) readings from JD 234 to JD 239 fluctuated between 4 and $20\,\mu g\,m^{-3}$. The mass concentrations from mid JD 240 to 252 were below $15\,\mu g\,m^{-3}$. A common feature found in the $PM_{2.5}$ time series is that the daily peak was always in the early afternoon. Similar patterns were not observed for other chemical variables around JD 231–232; the dramatic decrease of $PM_{2.5}$ mass at the beginning of the campaign was unclear.

The 30-min averaged SO_2 concentrations are shown in Fig. 3; distinct peaks were observed but not in a regular pattern such as the diurnal pattern found in the O_3 data (also shown in this figure). The daily peaks of ozone were observed usually in the early afternoon, consistent with the time when photochemical activity is at its peak, and mixing between the valley and the ridge top sampling site is usually vigorous.

The time series of the number concentrations [$dN/d\log(D_p)$ in # cm^{-3}] of 31, 41, and 51 nm particles are shown in Fig. 4 where N is the number concentration of particles, D_p is the mid-diameter of a size bin. Two large distinct peaks of these three particle size bins occurred in the afternoon of JD 236 and 237. There were also two smaller peaks, in comparison to these two huge ones, found in the afternoon of JD 240 and 241. Peaks of ultrafine particles were previously observed, but mostly in the early morning (Marti et al., 1997; Aalto et al., 2001) at Idaho Hill, Colorado. The peak heights shown in Fig. 4 are 11,000 at JD 236 on 1500 LST and 35,000 at JD 237 on 1800 LST for the 41-nm particles. This dramatic pattern repeats for 31- and 51-nm bins but not for other sizes, which showed more modest increases in the number concentrations. The changes of

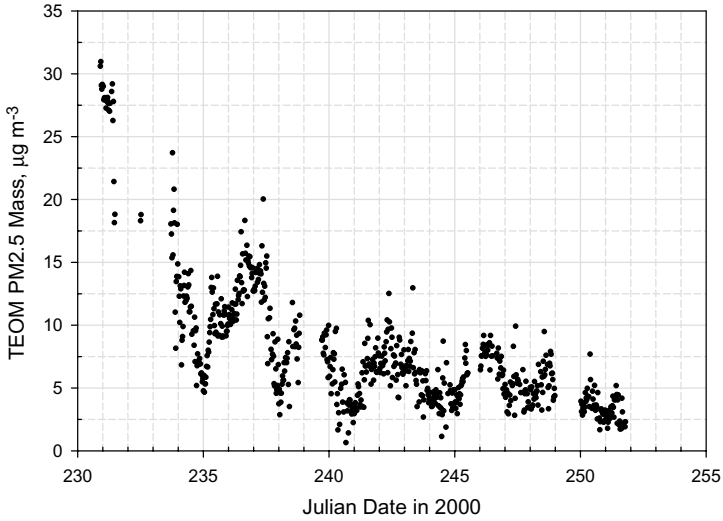

Fig. 2. A time-series plot of 30-min $PM_{2.5}$ mass concentration in units of $\mu g\,m^{-3}$ measured by TEOM.

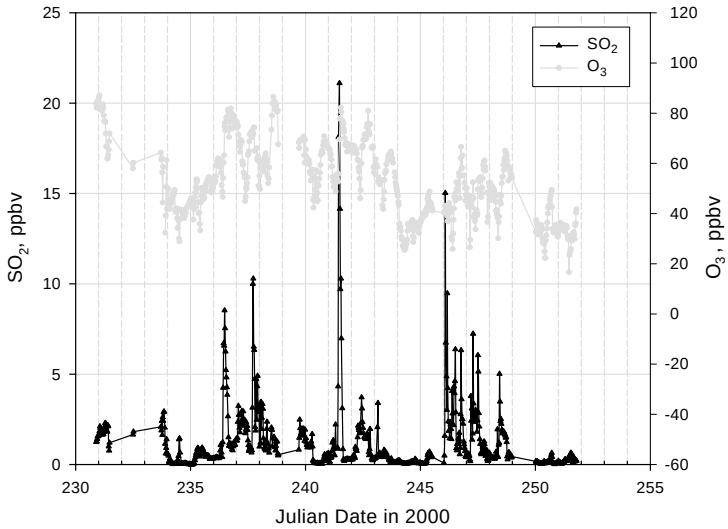

Fig. 3. A time-series plot of observed ozone and sulfur dioxide concentrations (both in ppbv) during the campaign.

particle number concentrations are less dramatic in JD 240 and 241 than those in JD 236 and 237.

The number concentrations of the accumulation-mode particles (101–626 nm) are shown in Fig. 5. The day-to-day variations of the diurnal cycle of Σ(101–200) and Σ(201–400) number concentrations were large. The peak of Σ(101–200) was found mostly at noon or late morning instead of in the afternoon. In contrast, and Σ(401–626) data were not as variable. There were elevated particle number concentrations found in between JD 235 and 239 that corresponds to the $PM_{2.5}$ pattern of these 4 days shown in Fig. 2. This finding is consistent with our regression analyses (see discussion below) indicating that $PM_{2.5}$ mass concentrations were better explained by Σ(101–200) and Σ(201–400) number concentrations than by Σ(401–626).

3.2. Factor analysis

Analyzing the variability in a large multivariate data set typically requires the use of a technique such as factor analysis. Interested readers are referred to Anderson (1984), for background material. This technique is commonly employed, for example, by receptor

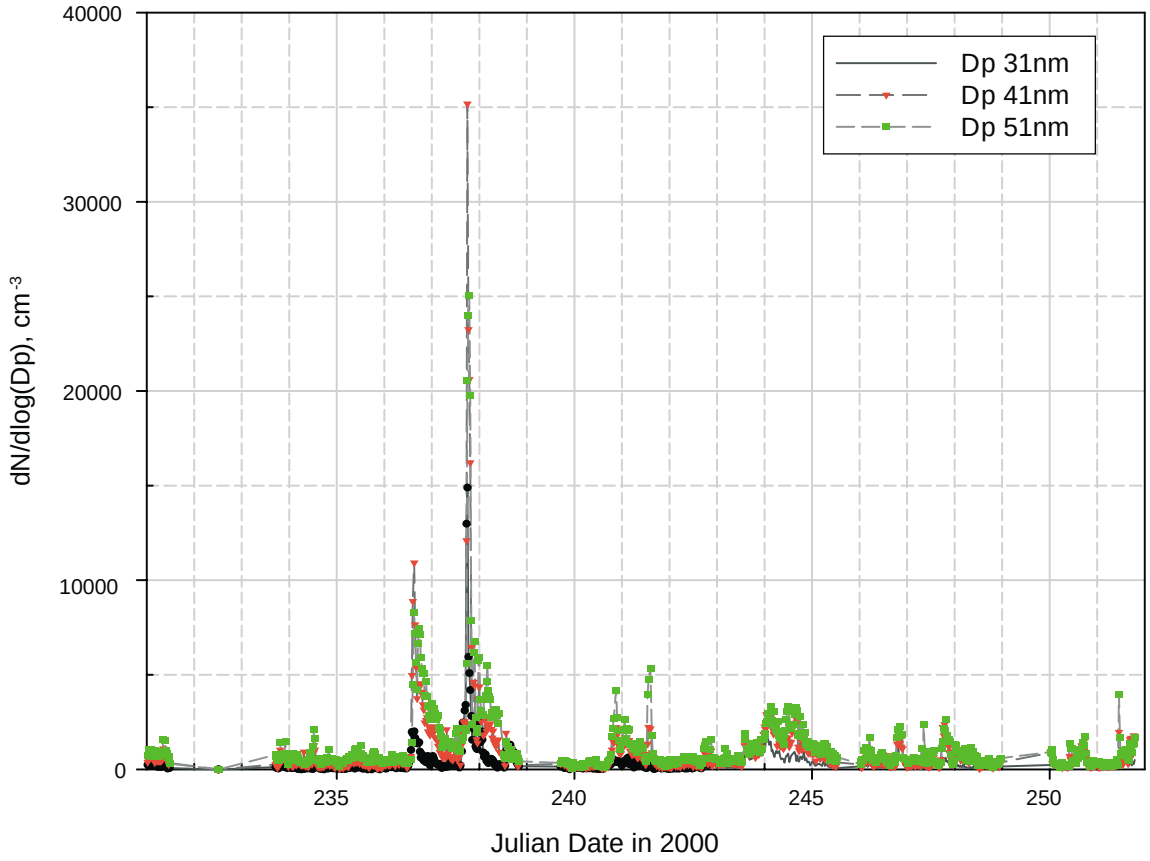

Fig. 4. A time-series plot showing the number concentrations (in # cm^{-3}) of particles of electrical mobility diameter of 31, 41, and 51 nm.

modelers to identify and quantify the contributions from particle emission sources (Hopke, 1985). In this study, we have applied the classical varimax-rotated factor analysis to explore this data set. Our intent was to resolve the complex relationships among the measured number concentrations as a function of particle size (from 10 to 626 nm), and with the concentrations of gaseous species and meteorological variables. It is important to note that the technique is designed to provide useful structural information regarding the relationships embedded in the data set.

A classical factor analysis using the varimax-rotation technique was performed using StatGraphics® for Windows® (version 4.0) on the 30-min averaged concentration data from JD230 to JD252. The eight summed number concentrations [Σ(15–30), Σ(31–40), Σ(41–50), Σ(51–60), Σ(61–100), Σ(101–200), Σ(201–400), Σ(401–626)], CO, NO_2, NO_y, O_3, SO_2, radiation, mean wind speed and $PM_{2.5}$ mass were used in the factor analysis.

As shown in Table 3, six (6) factors were resolved using this data set, in which each factor has an eigenvalue >1.0, the cutoff value chosen for distinguishing signal from noise embedded in the data. The 6-factor model accounts for 79.7% of the total variance embedded in the data (see column 4 of Table 3). Tests showed there to be no advantage in explaining the relationships among the 17 variables by including additional factors in the analysis.

The factor-loading matrix after the varimax-rotation is shown in Table 4 where significant loadings are in bold. The number concentrations of ultrafine mode particles (D_p, the electrical mobility diameter, from 15 to 100 nm) are grouped into Factor 1. The loadings for particles smaller than 60 nm were >0.8; the loading for Σ(61–100) was 0.71 also statistically significant. Statistically, this factor is independent of the gas variables (i.e., carbon monoxide, nitrogen species, ozone, and sulfur dioxide) included in the factor analysis. The reasons why variability in the concentrations of ultrafine particles ($D_p \leqslant 100$ nm) appears in a single factor are unclear at this point without, for example, additional data such as the chemical composition of the ultrafine particles. This issue should be pursued in future studies, especially if ultrafine particles are shown conclusively to cause adverse impacts to human health.

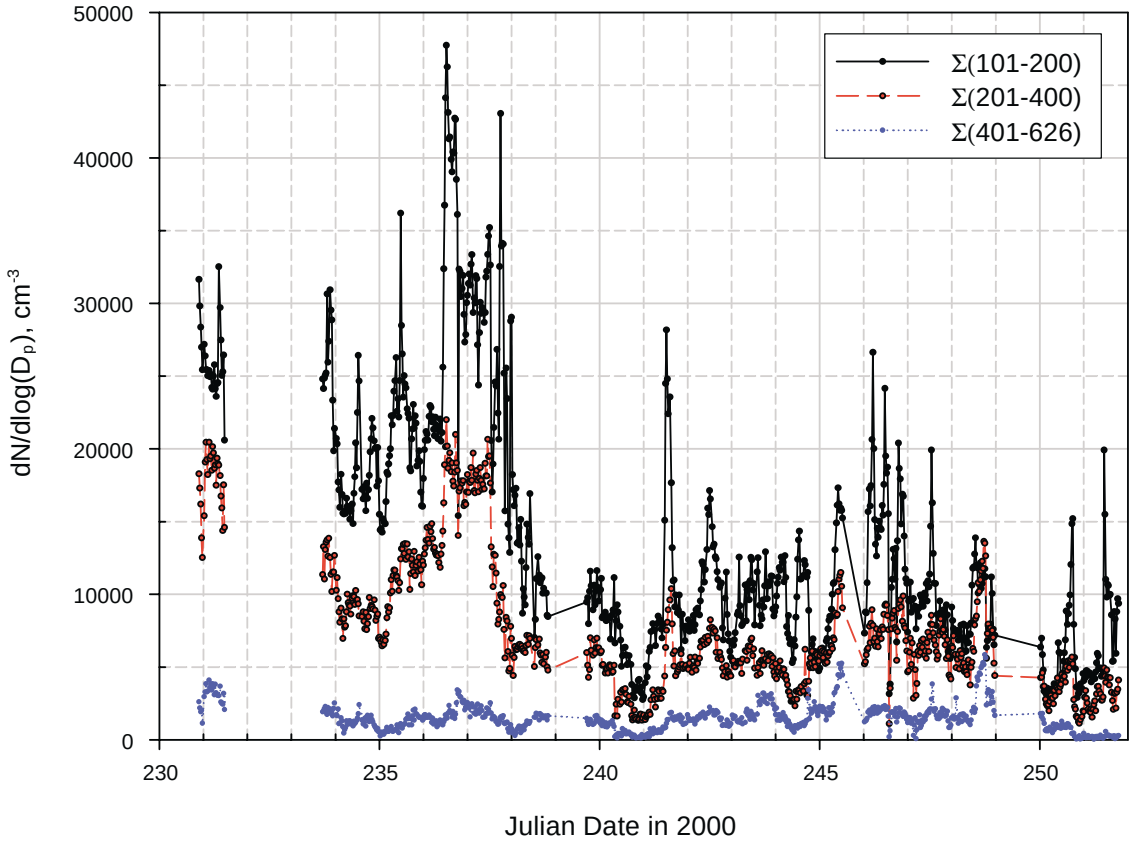

Fig. 5. A time-series plot of particle concentrations (in # cm^{-3}) of three summed size bins, Σ(101–200), Σ(201–400), and Σ(401–626).

Table 3
Eigenvalues of resolved data

Factor #	Eigenvalue	% variance	Cumulative % variance
1	**5.33**	**31.38**	**31.38**
2	**3.11**	**18.29**	**49.67**
3	**1.78**	**10.47**	**60.14**
4	**1.20**	**7.05**	**67.18**
5	**1.12**	**6.58**	**73.76**
6	**1.02**	**5.98**	**79.74**
7	0.77	4.52	84.27
8	0.73	4.28	88.54
9	0.51	3.00	91.55
10	0.50	2.93	94.48
11	0.32	1.91	96.39
12	0.24	1.43	97.82
13	0.19	1.13	98.94
14	0.09	0.51	99.45
15	0.05	0.31	99.76
16	0.03	0.20	99.96
17	0.01	0.04	100.00

Factor 2 has significant loadings in CO, Σ(101–200), Σ(201–400) and $PM_{2.5}$ mass (see column 3 of Table 4). $PM_{2.5}$ mass and number concentrations of accumulation-mode particles [i.e., Σ(101–200) and Σ(2011–400)] show up most strongly. The loading for CO was only 0.66—lower than that associated with particles. The variables, accumulation-mode particles, $PM_{2.5}$ and CO, are signatures for regional transport of pollutants. Based on these significant loadings, we assign this factor to regional transport. Ozone is known to be a regionally transported secondary pollutant, especially in summer and at higher altitudes, but its mean transport distance is not as large as secondary particles. Since its regional transport is not as dominant, it has a lower and statistically not significant loading on this factor.

Significant loadings of Factor 3 were found to be associated mainly with gaseous species that included NO_2 and NO_y, both of whose values were $\geqslant 0.8$. There was also a mild CO loading (0.51) and another smaller loading from SO_2 (0.59). Strong loadings in nitrogen species and a mild loading on SO_2 indicated that Factor 3 is associated with the primary gaseous emissions. These emissions likely include point and "immediate area" sources of NO_2, NO_y, and SO_2.

It was interesting that CO has mild loadings in Factor 2 (an assigned regional transport factor) and this Factor 3 (an assigned local primary emission factor).

Table 4
Factor loading matrix after varimax rotation

Variable	F1	F2	F3	F4	F5	F6	Communality
CO	0.00	**0.66**	0.51	0.12	0.09	−0.21	0.75
Mean wind speed	0.04	0.00	0.14	**0.85**	−0.09	0.01	0.75
NO	0.00	−0.06	0.05	−0.01	0.08	**0.95**	0.91
NO_2	0.17	−0.07	**0.91**	−0.09	−0.18	−0.01	0.90
NO_y	0.19	0.17	**0.81**	0.26	0.13	0.22	0.85
Ozone	0.15	0.48	0.00	**0.62**	0.24	−0.18	0.73
Radiation	−0.06	0.02	0.02	−0.03	**0.90**	0.09	0.82
SO_2	0.18	0.21	0.59	0.05	0.44	−0.09	0.63
Σ(101–200)	0.33	**0.86**	0.14	−0.05	0.06	−0.01	0.88
Σ(15–30)	**0.81**	−0.07	0.12	0.11	0.12	−0.06	0.71
Σ(201–400)	0.08	0.94	0.02	0.11	−0.01	0.02	0.91
Σ(31–40)	**0.94**	−0.02	0.08	0.06	0.04	−0.04	0.90
Σ(401–600)	−0.02	0.49	−0.06	0.44	−0.03	0.20	0.48
Σ(41–50)	**0.96**	0.06	0.06	0.03	−0.05	0.00	0.92
Σ(51–60)	**0.91**	0.13	0.10	0.00	−0.10	0.04	0.86
Σ(61–100)	**0.71**	0.41	0.21	−0.09	−0.04	0.07	0.73
$PM_{2.5}$ mass	−0.06	**0.90**	0.03	0.08	0.03	−0.06	0.82

Tropospheric CO mixing ratios are ranging from 40 to 200 ppbv (p. 86, Seinfeld and Pandis, 1998). However, the minimum and maximum CO values observed in our campaign were 79 and 441 ppbv, respectively (Table 2), with a median of 169 ppbv. The median concentration of our CO data is at the higher end of the mixing ratio range reported by Seinfeld and Pandis (1998). Note that ozone is completely absent (loading = 0.00) in Factor 3, and that neither the particle number concentrations nor $PM_{2.5}$ mass has significant loadings. Hence, variability in primary gaseous emissions including point sources and mobile sources in the Knoxville area could be the primary contributing sources of Factor 3.

A significant loading in Factor 4 includes mean wind speed (loading = 0.85). A mild loading (0.62) was calculated for ozone. This loading pattern suggests that variability in the 30-min mean wind speed could not explain any variability of the particle variables. The ability to use mean wind speed to explain ozone variation was moderate as seen in the loading values. As previously discussed for Factor 2, ozone is a secondary species transported over a sub-regional scale compared to secondary particles (in the accumulation mode). In Factor 4, ozone was decoupled from particle loadings and other primary gaseous emissions. Since mean wind speed was the single "statistically" significant factor loading, this factor was assigned as a unique factor of mean wind transport, possibly responsible for the ozone variation observed at the site.

A single strong loading for Factor 5 is solar radiation (loading = 0.90). Note that although the loading for SO_2 on Factor 5 was 0.44, the second largest on this factor, this loading is statistically insignificant. With the low factor signal on SO_2 and all other variables except solar radiation, we attribute this factor to the variation of solar variation alone.

Interestingly, NO (loading = 0.95) was the single significant loading on Factor 6. We think that this was associated with the data quality of this particular variable. Note that from Table 2 the data recovery rate for this variable was 48%, about 30% lower than other variables. Thus, it is likely this factor simply isolate the variable from others and we should attribute this factor as a unique factor meaning it could not be explained by any physical relationships with other variables we have included.

3.3. Multivariate correlation of $PM_{2.5}$ mass concentration with gaseous and particulate variables

We have performed a multiple linear regression of $PM_{2.5}$ mass on CO, O_3, NO, NO_2, NO_y, SO_2, and particle number concentrations of the eight summed size bins. This regression was performed independent of the factor analysis and was served for the purpose of variable selection for identifying major contributing variables to $PM_{2.5}$ mass. The regression result is shown in Table 5. The r^2 value for this regression was 0.74. The statistically significant (non-zero) variables found in this regression were the intercept, O_3, CO, and particles from 0.1 to 0.4 μm. This finding is consistent with the factor analysis results presented earlier. A statistically significant variable was one whose P value was smaller than 0.05 or a 95% confidence interval. Ultrafine particles smaller than or equal to 100 nm did not contribute to the observed 30-min averaged $PM_{2.5}$ mass, nor the particles >400 nm in diameter that also contributed little to $PM_{2.5}$ mass.

Table 5
Linear regression of $PM_{2.5}$ mass (measured by TEOM) on selected gaseous and particulate variables

$PM_{2.5}$ mass ($\mu g\,m^{-3}$) =	Estimate	Standard error	*T*-statistics	*P*-value
Constant	−5.49E + 00	9.11E−01	−6.02**	0.00
CO, ppbv	3.53E−02	5.41E−03	6.52**	0.00
NO, ppbv	−3.17E−01	4.21E−01	−0.75	0.45
NO_2, ppbv	1.76E−01	3.17E−01	0.56	0.58
NO_y, ppbv	−6.12E−02	1.56E−01	−0.39	0.69
O_3, ppbv	5.79E−02	1.61E−02	3.59**	0.00
SO_2, ppbv	−3.45E−02	8.20E−02	−0.42	0.67
Σ(15–30), # cm^{-3}	7.24E−05	1.36E−04	0.53	0.60
Σ(31–40), # cm^{-3}	−8.29E−05	1.45E−04	−0.57	0.57
Σ(41–50), # cm^{-3}	9.39E−05	1.75E−04	0.54	0.59
Σ(51–60), # cm^{-3}	−9.93E−05	1.60E−04	−0.62	0.54
Σ(61–100), # cm^{-3}	3.49E−05	6.34E−05	0.55	0.58
Σ(101–200), # cm^{-3}	−1.88E−04	5.96E−05	−3.16**	0.00
Σ(201–400), # cm^{-3}	9.25E−04	9.81E−05	9.43**	0.00
Σ(401–626), # cm^{-3}	−1.14E−04	1.85E−04	−0.62	0.54

Note: r^2 of this regression is 0.74. Particles in the size range of 0.1–0.4 μm are statistically correlated with $PM_{2.5}$ mass; however, the sign for 0.1–0.2 μm was negative possibly indicating particle growth (lost) into the next size bin. CO and O_3 were also significant in predicting $PM_{2.5}$ mass concentration.

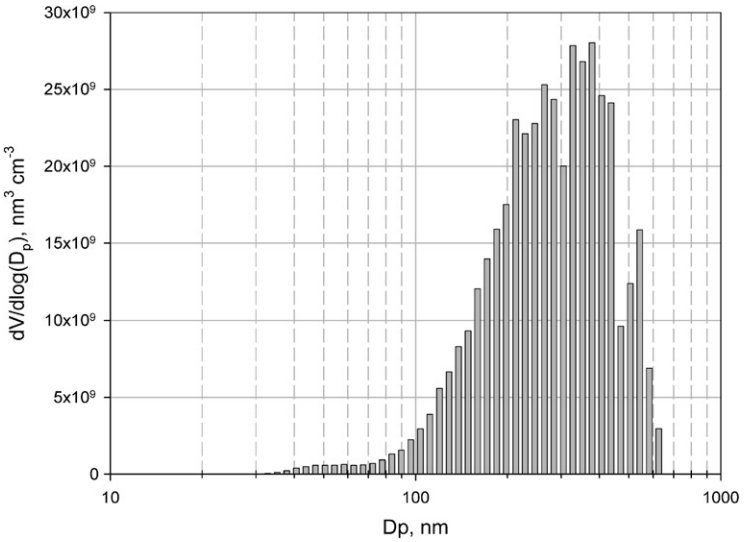

Fig. 6. A plot of particle volume distribution as a function of mid-point diameter of each size bin. The units for the *y*-axis are $nm^3\,cm^{-3}$ and for the *x*-axis is nm.

Fig. 6 shows a typical example (as commonly seen in our data) of the distribution of particle volume as a function of the mobility diameter observed around 1300 LST on 23/08/2000. The distribution appears to be lognormal but right-skewed with a long tail extending left into the ultrafine size range. The volume distribution shown in Fig. 6 has a peak diameter around 320 nm. The volumes of particles >400 nm in size appeared to be insignificant as compared to that in the 100–400 nm size range. Since particle volume is proportional to particle mass, observation of such distributions throughout the campaign further supports the multiple regression results. In other words, most of the $PM_{2.5}$ mass concentrations measured at the site could be attributed to particles in the diameter range from 0.1 to 0.4 μm, much less to the ultrafine and not to those >400 nm.

4. Conclusions

A varimax-rotation factor analysis was performed to explore the relationship of the fine and ultrafine particle number concentrations, the gaseous species concentration, the mean wind speed, and the solar radiation. A

6-factor model was found to best resolve 79.7% of the variability embedded in the data. The model suggests that 31.4% of the data variability could be explained by ultrafine particles (the diameters smaller than or equal to 100 nm). It was difficult to further elucidate this factor without chemistry information of the ultrafine particles. However, no gas species were loaded on Factor 1, indicating that ultrafine particle concentrations observed in this study were not associated with primary source emissions of NO_x and SO_2. The decoupling of the ultrafine particles from the fine particles also implies that the former ones might have been produced and transported to the site by separated mechanisms from those of fine particles. The second factor included the $PM_{2.5}$ mass concentration and the number concentrations of particles in the diameter range of 101–400 nm. The loading pattern on Factor 2 led to the conclusion that this factor was contributed by regional transport. The third factor includes CO, NO_2, reactive odd nitrogen (NO_y), and SO_2 that were contributed by primary source emissions. The mean wind speed and ozone (with a mild loading) were loaded in Factor 4 that was tentatively labeled as mean wind transport. Identification of this factor led to an observation that ozone transport to the site may be in part decoupled from the regional transport factor of fine particles (i.e., Factor 2). Solar radiation was singly included in the fifth factor indicating this is a unique factor. The quality of NO data was marginal and this variable was placed by the model into Factor 6. A multiple regression analysis further indicated that $PM_{2.5}$ mass concentration was best explained by CO, O_3, and number concentrations of particles in the diameter range between 0.1 and 0.4 μm. Most of the $PM_{2.5}$ mass concentrations measured at the site could be attributed to particles in the diameter range from 0.1 to 0.4 μm, much less to the ultrafine and nor to those >400 nm.

We also observed interesting change in the particles of size from 31- to 51-nm range. Two unique events were identified during the campaign in which the number concentrations of 31–51 nm particles dramatically increased by a factor of 10 in 30 min, reaching 40,000 cm^{-3}, with the peaks lasting for a couple of hours. Particles in the adjoining size ranges also exhibited increases, albeit more modest, during these events.

Acknowledgements

The authors acknowledged the assistance of Thomas Wainman of the Oak Ridge Associated Universities and Solomon Bairai, Elizabeth Gray, Ken Olszyna, David Phillips, Larry Shelton, Myra Valente, Ray Valente, and Mark Wolfe of TVA in acquiring the data. Thomas Wainman was supported in part by an appointment to the ORNL Postdoctoral Research Associates Program administered jointly by the ORNL and the Oak Ridge Institute for Science and Education. The DOE/Fossil Energy/Natural Gas and Oil Technology Program, DOE's National Energy Technology Laboratory, EPRI, and TVA's Public Power Institute provided partial funding of this work. The authors acknowledge the thorough and in-depth comments of two anonymous reviewers who helped improve the quality of this manuscript. Oak Ridge National Laboratory is managed by UT-Battelle, LLC, for the US Department of Energy under contract DE-AC05-00OR22725.

Disclaimer

The mention of trade names, instruments, and/or chemicals in this paper does not imply the endorsement from the authors.

References

Aalto, P., Hameri, K., Becker, E., Weber, R., Salm, J., Makela, J.M., Hoell, C., O'Dowd, C.D., Karlsson, H., Hansson, H.C., Vakeva, M., Koponen, I.K., Buzorius, G., Kulmala, M., 2001. Tellus B 53 (4), 344–358.

Anderson, T.W., 1984. An Introduction to Multivariate Statistical Analysis, 2nd Edition.. Wiley, New York.

Clarke, A.D., 1992. Atmospheric nuclei in the remote free troposphere. Journal of Atmospheric Chemistry 14, 479–488.

Ding, Y.M., Pang, Y.B., Eatough, D.M., Eatough, N.L., Tanner, R.L., 2002. High-volume diffusion denuder sampler for the routine monitoring of fine particulate matter: II. Field evaluation of the PC-boss. Aerosol Science and Technology 36, 383–396.

Flagan, R.C., Wang, S.-C., Yin, F., Seinfeld, J.H., Reischl, G., Winklmayr, W., Karch, R., 1991. Electrical mobility measurements of fine-particle formation during chamber studies of atmospheric photochemical reactions. Environmental Science and Technology 25, 883–890.

Heisler, S.L., Friedlander, S.K., 1977. Gas-to-particle conversion in photochemical smog: aerosol growth laws and mechanisms for organics. Atmospheric Environment 11, 157–168.

Hopke, P.K., 1985. Receptor Modeling in Environmental Chemistry. Wiley, New York, NY.

Kulmala, M., Hämeri, K., Aalto, P.P., Mäkelä, J.M., Pirjola, L., Nilsson, E.D., Buzorius, G., Rannik, Ü., Dal Maso, M., Seidl, W., Hoffman, T., Janson, R., Hansson, H.-C., Viisanen, Y., Laaksonen, A., O'Dowd, C.D., 2001. Overview of the international project on biogenic aerosol formation in the boreal forest (BIOFOR). Tellus 53B (4), 324–343.

Marti, J.J., Weber, R.J., McMurry, P.H., Eisele, F., Tanner, D., Jefferson, A., 1997. New particle formation at a remote continental site: assessing the contribution of SO_2 and organic precursors. Journal of Geophysical Research—Atmosphere 102, 6331–6339.

McMurry, P.H., Friedlander, S.K., 1979. New particle formation in the presence of an aerosol. Atmospheric Environment 13, 1635–1651.

Modey, W.K., Pang, Y., Eatough, N.L., Eatough, D.J., 2001. Fine particulate ($PM_{2.5}$) composition in Atlanta, USA: assessment of the particle concentration-Brigham Young University Organic Sampling System, PC-BOSS, during the EPA supersite study. Atmospheric Environment 35, 6493–6502.

Peters, A., Wichmann, H.E., Tuch, T., Heinrich, J., Heyder, J., 1997. Respiratory effects are associated with the number of ultrafine particles. American Journal of Respiratory and Critical Care Medicine 155, 1376–1383.

Pirjola, L., Laaksonen, A., Aalto, P., Kulmala, M., 1998. Sulfate aerosol formation in the arctic boundary layer. Journal of Geophysical Research 103, 8309–8322.

Seinfeld, J., Pandis, S., 1998. Atmospheric Chemistry and Physics. Wiley, New York, NY.

Tanner, R.L., Parkhurst, W.J., 2001. Sources of PM2.5 carbonaceous aerosols at a site near the Great Smoky Mountains National Park, Poster paper presented at the 20th National Meeting of the American Association for Aerosol Research held in Portland, OR, in October.

Wehner, B., Wiedensohler, A., Heintzenberg, J., 2000. Submicrometer aerosol size distributions and mass concentration of the millennium fireworks 2000 in Leipzig, Germany. Journal of Aerosol Science 31, 1489–1493.

Woo, K.S., Chen, D.R., Pui, D.Y.H., McMurry, P.H., 2001. Measurement of Atlanta aerosol size distributions: observations of ultrafine particle events. Aerosol Science and Technology 34, 75–87.